ICARUS 117, 435–438 (1995)

NOTE

Formation of Isolated Narrow Ringlets by a Single Satellite

J. HÄNNINEN[1] AND H. SALO[2]

Department of Astronomy, University of Oulu, FIN-90570 Oulu, Finland
E-mail: jyrki@seita.oulu.fi

Received June 10, 1994; revised May 24, 1995

The generation of the density wave trains at the satellite resonance zones of the dense planetary rings is qualitatively understood (e.g., F. Shu, 1984, in *Planetary Rings*, pp. 513–561, Univ. of Arizona Press, Tucson, AZ), but the optically thin C-ring and the Cassini Division behave drastically differently: in some of the resonance locations isolated narrow ringlets are found, often embedded in a gap (G. L. Tyler *et al.*, 1983, *Icarus* 54, 160–188). According to our numerical *N*-body simulations a single satellite can create a narrow ringlet with sharp outer and inner edges. In the experiments with a bimodal size distribution the large particles become more efficiently confined, in agreement with the observations where the fraction of small particles is found to be enhanced at the ringlet edges (Tyler *et al.* 1983).

Even if the rings of Saturn consist of thousands of smaller ringlets, there are only few truly isolated ringlets with adjacent empty gaps (optical depth $\tau < 0.01$), located in the low-density C-ring and the Cassini Division ($\tau \approx 0.1$) (Tyler *et al.* 1983). Many of these narrow ringlets (with typical widths of a few tens of kilometers) are found in the isolated resonance locations of different satellites. Their edges are extremely sharp: in several cases τ drops to zero within radial distance of 1 km. For example, the Prometheus 2:1 inner Lindblad resonance (2:1 ILR) is located at the distance of 88,713.7 km. At the same radius a ringlet is found, embedded in an empty gap (also the Mimas 3:1 inner vertical resonance falls at the ringlet, but its strength is an order of magnitude weaker) (Porco and Nicholson 1987, Rosen *et al.* 1991). There exists also resonances without ringlets and ringlets without any connection to the known satellite resonances (Cuzzi *et al.* 1984).

The standard theoretical explanation for the resonance features relies on the satellite torque exerted on the resonance zone: at the ILR angular momentum is removed from the ring, leading to opening of a gap just outside the ILR, provided that the satellite torque exceeds the viscous torque due collisions which tend to smooth all density variations (Goldreich and Tremaine 1978). The extreme sharpness of the inner gap boundary results from the reversal of viscous flux near the ring edge due to satellite-induced streamline distortion (Borderies *et al.* 1989). However, the formation of an isolated ringlet with a sharp inner and outer edge is more problematic, as the standard theory provides no mechanism to prevent the diffusion of the inner edge. For example, in the case of Saturn's F-ring and the narrow uranian rings, pairs of confining shepherding satellites have been evoked (Goldreich and Tremaine 1979), the sharp inner edge being explained by the other Lindblad resonance (OLR) of another satellite orbiting interior to the ringlet. This explanation is clearly not applicable for Saturn's C-ring ringlets where several isolated ringlets without shepherding moons are found at ILR locations.

As an adequate theoretical explanation for the ringlets is missing we turn into numerical simulations. This allows, in addition to the study of the ringlet formation, also an extension of the theoretical linear torque estimates for the highly nonlinear density variations. In the present Note we concentrate on the 2:1 ILR and study it in terms of direct three-dimensional collisional simulations, both with identical particles and with a bimodal size distribution. As self-gravity is not likely to be important in the C-ring (Salo 1992), we use massless test particles. Schwarz (1981) has also simulated 2:1 ILRs: compared to his experiments, the present simulations have about 50-fold duration, employ an accurate calculation of the individual impacts between finite size particles, and use simulation parameters obtained by careful scaling of the physical satellite–ring parameters.

In the simulations isolated ringlets with adjacent gaps form just inside the 2:1 ILR location for sufficiently large satellites (Fig. 1). The limiting satellite mass for the gap formation agrees with the standard linear theory (Goldreich and Tremaine 1982; see also Hänninen and Salo 1992). Initially, spiral density wakes appear at the resonance, increasing gradually in strength and finally transforming to a narrow steady-state ringlet, embedded in a practically empty gap. At the ringlet stage, velocity dispersion has attained a constant value.

The initial and final density profiles of the simulation of Fig. 1 are plotted at Fig. 2a. Besides the sharp edges of the ringlet, a typical feature is the more prominent outer gap than the inner one. Figure 2b displays the final density profile of the simulation with a bimodal size distribution. The population of the larger particles has formed a ringlet, while the smaller ones have become more dispersed, leading to a relative excess of smaller particles at the ringlet edges. Similar excess has been observed at the narrow ringlets of the C-ring (Tyler *et al.* 1983).

Figure 3 displays the decrease of the ring angular momentum I (dashed lines show ΔI multiplied by Ω, the angular frequency at the resonance radius), its slope being proportional to the instantaneous satellite torque. The two different stages of the evolution are visible: (1) during the spiral wake stage the satellite exerted torque is proportional to $T_s \sim (M_s/M_p)^2\tau_o$, while (2) when the wake transforms to a ringlet, there is an abrupt change in the slope, to $T_s \sim M_s/M_p\tau_o^q$ with $q \simeq 1.5$. The observed wake stage torque has the same optical depth and satellite mass dependence as predicted by the standard formula (Goldreich and Tremaine 1982) of linear T_s, although its magnitude is about two-fold as compared to linear theory. On the other hand, the $\tau_o^{1.5}$-dependence of the ringlet

[1] Current address: LPL, University of Arizona, Tucson, AZ 85721.
[2] Current address: Instituto de Astronomia, UNAM, Mexico, DF.

0019-1035/95 $12.00

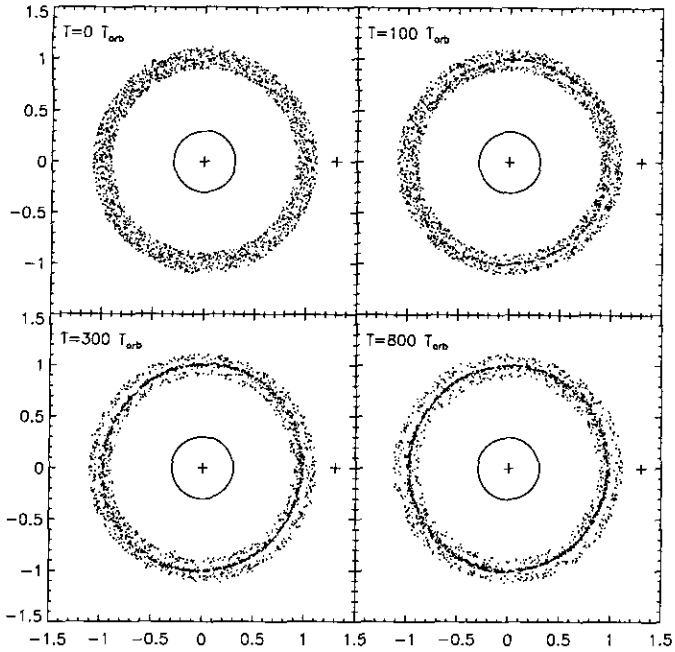

FIG. 1. Time evolution of a collisional ring with 2000 spherical, frictionless, and massless particles with a radius $\sigma = 0.001$ and an initial optical depth $\tau_o = 0.01$. The ring is perturbed with a satellite of mass $\mu_s = M_s/M_p = 8.871 \times 10^{-5}$ on a circular orbit, 2:1 ILR falling on the unit distance. The satellite position is marked by the cross, but not in correct radial scale. The initial width of the system is 0.05: in the plot the ring width is multiplied by a factor of two. The integration algorithm (Hänninen and Salo 1992, Hänninen 1993) is based on Aarseth's N-body integrator (Aarseth 1985) which uses a fourth-order force polynomial and an individual time-step scheme in the integration of particle orbits. The standard impact model is used with the Bridges *et al.* (1984) velocity-dependent coefficient of restitution for ice particles $\varepsilon(v) = (v_n/v_c)^{-0.234}$, where v_n is the perpendicular component of the relative velocity and the constant $v_c \approx 0.01$ cm/sec. In the numerical experiments the particle size is necessarily much larger than true size, if realistic values of optical depth are simulated. Therefore, to be able to compare the results to realistic systems, various parameters have been appropriately scaled. First of all, we want to maintain the relative importance of the finite particle size in determining the unperturbed equilibrium velocity dispersion. This is achieved by adjusting the parameter v_c so that $\sigma\Omega/v_c$, where Ω is angular frequency at 2:1 ILR, is constant (Salo 1991). For 1-m particles in the C-ring at the Prometheus 2:1 ILR, we thus adopt $v_c = 4.2891 \times 10^{-4}$. Similarly, to keep the ratio between satellite induced velocities and nonperturbed velocities constant, satellite mass is scaled proportional to v_c (or $\sigma\Omega$) (Hänninen and Salo 1994). Therefore the simulation mass $\mu_s = 8.871 \times 10^{-5}$ corresponds to the physical mass $\mu_{ph} = 1.0 \times 10^{-9}$.

torque is weaker than the theoretical nonlinear estimate $\sim\tau_o^2$ (Borderies *et al.* 1984). The difference during the wake stage follows from the density perturbation being already quite substantial and continuously increasing: the difference with the linear theory vanishes with small satellite masses generating only negligible density enhancement. The reduced torque at the ringlet stage, as compared to that at the wake stage, follows from the negative torque being partially compensated by the positive torque exerted on the inner half of the ringlet (Hänninen and Salo 1994).

Figure 3 shows also the evolution of the ring total energy (solid line), following closely the $\Omega\Delta I$ curve. This coupled evolution can be understood as follows. The work (negative in ILR) done by the satellite is related to the torque by $dE_s/dt = \Omega_s T_s$, where Ω_s stands for the satellite angular frequency. Conservation of the Jacobi constant for the individual orbits between the impacts requires that the satellite-induced increase of the random kinetic energy, dE_{kin}/dt, is related to the work by Dermott (1984), $dE_{kin}/dt = (1 - \Omega/\Omega_s)\, dE_s/dt$. If the collisional dissipation exactly cancels the induced eccentricities (as is observed in the present simulations during the ringlet stage as the velocity dispersion stays constant), $dE_{coll}/dt + dE_{kin}/dt = 0$, this leads to dissipation rate,

$$\frac{dE_{coll}}{dt} = (\Omega - \Omega_s) T_s, \tag{1}$$

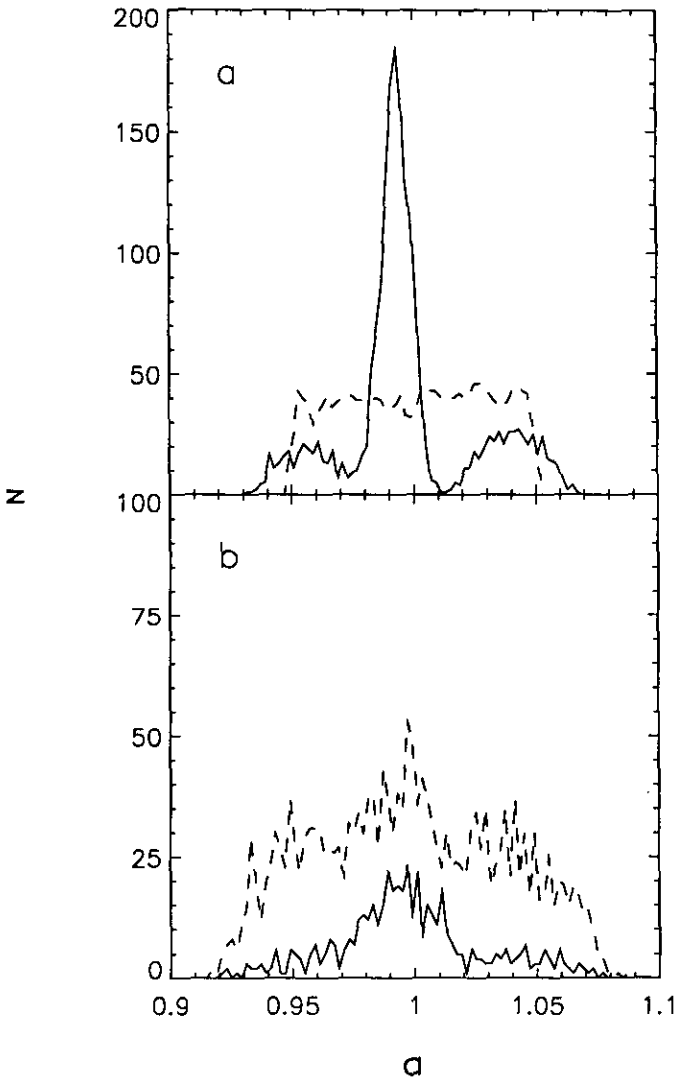

FIG. 2. (a) Radial density profile of the ring at the beginning ($t = 0\ T_{orb}$; dashed line) and at the end ($t = 800\ T_{orb}$; solid line) of the simulation of Fig. 1. (b) Density profile at the end ($t = 800\ T_{orb}$) of a simulation with a bimodal size distribution (500 large particles with $\sigma = 0.002$ and 2000 particles with $\sigma = 0.001$). The solid line stands for the distribution of the large particles and the dashed line for the distribution of the small ones. The initial optical depth of the both populations is $\tau_o = 0.01$.

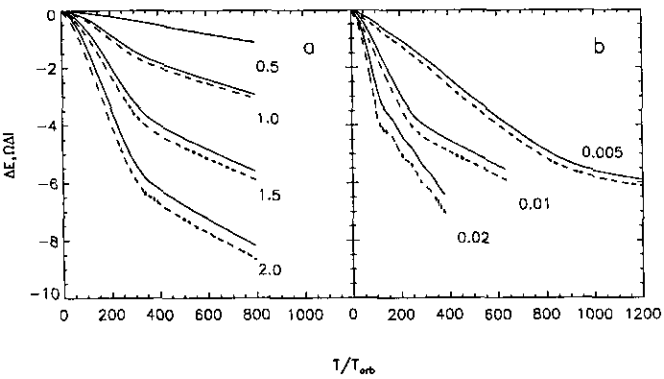

FIG. 3. The observed change in the ring total angular momentum ΔI multiplied by Ω (dashed line), its slope being proportional to instantaneous satellite torque, displayed together with the cumulative change in the ring total energy ΔE (solid line). In the initial state $I = 2000$ and $E = -1000$. In (a) the angular momentum change is compared between different satellite masses (the satellite masses are $\mu_{ph} = 0.5 \times 10^{-9}$, 1.0×10^{-9}, 1.5×10^{-9}, and 2.0×10^{-9}) with same initial $\tau_o = 0.01$. In (b) the comparison is done between different initial optical depths ($\tau_o = 0.005, 0.01$, and 0.02), but for the same satellite mass $\mu_{ph} = 2 \times 10^{-9}$.

and to total energy decrease,

$$\frac{dE}{dt} = \frac{dE_s}{dt} + \frac{dE_{\text{coll}}}{dt} = \Omega T_s. \tag{2}$$

For the final ringlet stage the slopes of the angular momentum and energy curves are practically equal, indicating a balance between the energy dissipation and external torque (notice that since most of the particles are at the dense ringlet, dissipation and torque outside the ringlet are insignificant). On the other hand, during the wake stage when the ringlet is still forming, $|dE/dt| < |\Omega T_s|$ as collisional dissipation is unable to balance the work connected to the satellite torque.

It is well known that an unperturbed ring experiences radial spreading due to collisional diffusion (Brahic 1977). On the macroscopic level this follows from the conservation of ringlet's angular momentum while its total energy decreases. Assume a narrow ringlet with a uniform surface density, mean distance $\bar{a}$, and width $W \ll \bar{a}$. The ringlet energy and angular momentum are $E = -GM_pM_R/(2\bar{a})$ and $I = \sqrt{GM_p\bar{a}}M_R(1 + 1/32(W/\bar{a})^2)$, respectively, where M_R is the ringlet mass and G stands for the gravitational constant. These equations hold also for a gaussian surface density profile if W^2 is replaced by $12\delta^2(a)$, where $\delta(a)$ stands for the dispersion of semimajor axis. Defining $f_c = \Omega\Delta I/\Delta E$, the changes in $\bar{a}$ and W are connected by

$$\frac{\Delta W}{\Delta \bar{a}} = \frac{8\bar{a}}{W}\left(f_c - 1 + \frac{3}{32}\left(\frac{W}{\bar{a}}\right)^2\right). \tag{3}$$

For a nonperturbed ringlet $f_c = 0$, so that

$$\frac{dW}{dt} \simeq -\frac{8\bar{a}}{W}\frac{d\bar{a}}{dt}. \tag{4}$$

As $d\bar{a}/dt = 2\bar{a}^2/(GM_pM_R)dE/dt$ is negative, narrow ringlets should expand rapidly.

Both the rapid initial contraction of the system during the wake stage, and the apparent confinement of the final ringlet can be qualitatively understood with the help of Eq. (3). During the wake stage the observed $f_c \approx 1.1$, which value inserted into Eq. (3) implies $\Delta W \approx \Delta\bar{a}(\bar{a}/W)$, in accordance with the rapid contraction. However, this is just a macroscopic interpretation for what is observed; in the microscopic level the most likely explanation is the reversal of the angular momentum flux in collisions, due to the strong streamline perturbation, turning the viscous expansion into contraction with the approximately same time scale (see eg. Borderies *et al.* 1984).

During the final ringlet stage, the observed values $f_c \approx 0.99 \pm 0.01$ which indicates a strongly reduced expansion rate as compared to the expansion of a similar isolated ringlet. Within the accuracy attainable in the present simulations, this agrees with the observed practically constant ringlet width. Formally, f_c of exactly unity in Eq. (3) would imply a slow contraction, but as f_c is a zero-order quantity and $(W/\bar{a})^2 \sim M_s/M_p$ (identifying W with the width of the resonance zone), neglecting $f_c - 1$ with respect to $(W/\bar{a})^2$ is not justified, as noted by Goldreich (1994, private communication). Again, this interpretation in terms $f_c \approx 1$ is just a qualitative description of the observed macroscopic behavior. In the microscopic level the observed confinement most probably follows from the angular momentum luminosity $L_H(a)$ vanishing throughout the entire ringlet once it has attained a large enough optical depth (Goldreich 1994; see also Borderies *et al.* 1984, and Goldreich and Porco 1987).

In the case of a bimodal size distribution the particle populations interact with each other, the large particles supplying random kinetic energy to the smaller ones. Figure 4 displays the cumulative ΔE and $\Omega\Delta I$ in the experiment with a bimodal size distribution, already studied in Fig. 2b. Due to the collisions with the large particles, the population of the smaller particles is not able to balance its energy loss against the satellite-exerted torque, and thus their $f_c < 1$. The larger particles, on the other hand, have a much better balance ($f_c \approx 1$), because the collisions with the small particles have only a weak effect on their energy budget. This offers a qualitative macroscopic interpretation for the observed expansion and contraction of the smaller and larger particles, respectively.

According to above numerical experiments a single satellite can create and maintain a narrow isolated ringlet in its ILR. However, due to the inward drift caused by the collisional dissipation, this offers only a temporary mechanism for the confinement. The time scale for the drift across the resonance zone $T_{\text{life}} \approx W_{\text{res}}/\dot{\bar{a}}$, where $W_{\text{res}} \simeq \sqrt{M_s/M_p}a$ stands for the width of the resonance zone. Now $\dot{\bar{a}} \propto \dot{E} \propto \omega_c c^2$, where the impact frequency ω_c is proportional to τ and the velocity dispersion c to σ. For the simulation with $M_s/M_p = 8.87 \times 10^{-5}$, $\tau_o = 0.01$, and $\sigma/a = 0.001$ the observed drift speed yields $T_{\text{life}} \simeq 2100$ orbital periods. Scaling to realistic satellite masses ($M_s/M_p = 1 \times 10^{-9}$), particle sizes ($\sigma = 1$ m), and optical depths ($\tau_0 = 0.1$) gives $T_{\text{life}} \approx 7 \times 10^9$ orbital periods, or about

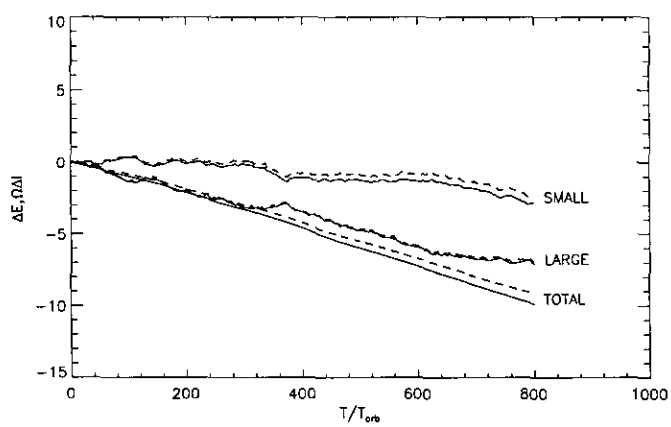

FIG. 4. The observed change in the ring angular momentum ΔI (multiplied by Ω; dashed line) and total energy ΔE (solid line) is displayed for the simulation with a bimodal size distribution (see Fig. 2b).

8×10^6 years for the Prometheus 2:1 ILR ringlet. This is comparable to the estimated time scale for the recession of Prometheus from the A-ring outer boundary to its present location (Borderies *et al.* 1984). In Saturn's C-ring the gradual drift from the resonance could also be affected by the mass flow from the unperturbed region: modeling this diffusion is, however, outside the scope of the present simulations. As the simulated mechanism also works for OLRs, the narrow core of Saturn's F-ring might also be confined solely by Prometheus, the inner more massive and closer satellite. The same type of mechanism might also be at work in the uranian ring system.

ACKNOWLEDGMENT

We thank Dr. P. Goldreich for illuminating discussions and criticism.

REFERENCES

AARSETH, S. J. 1985. Direct methods for N-body simulations. In *MultipleTime Scales* (J. E. Brackbill and B. I. Cohen, Eds.), pp. 377–418. Academic Press, Orlando, FL.

BORDERIES, N., P. GOLDREICH, AND S. TREMAINE 1984. Unsolved problems in planetary ring dynamics. In *Planetary Rings* (R. Greenberg and A. Brahic, Eds.), pp. 713–734. Univ. of Arizona Press, Tucson.

BORDERIES, N., P. GOLDREICH, AND S. TREMAINE 1989. The formation of sharp edges in planetary rings by nearby satellites. *Icarus* **80,** 344–360.

BRAHIC, A. 1977. Systems of colliding bodies in a gravitational field. I. Numerical simulations of the standard model. *Astron. Astrophys.* **54,** 895–907.

BRIDGES, F. G., A. HATZES, AND D. N. C. LIN 1984. Structure, stability and evolution of Saturn's rings. *Nature* **97,** 333–335.

CUZZI, J. N., J. J. LISSAUER, L. W. ESPOSITO, J. B. HOLBERG, E. A. MAROUF, G. L. TYLER, AND A. BOISCHOT 1984. Saturn's rings: ties and processes. In *Planetary Rings* (R. Greenberg and A. Brahic, Eds.), pp. 73–199. Univ. of Arizona Press, Tucson.

DERMOTT, S. F. 1984. Dynamics of narrow rings. In *Planetary Rings* (R. Greenberg and A. Brahic, Eds.), pp. 589–637. Univ. of Arizona Press, Tucson.

GOLDREICH, P., AND C. PORCO 1987. Shepherding of the Uranian rings. II. Dynamics. *Astron. J* **93,** 730–737.

GOLDREICH, P., AND S. TREMAINE 1978. The formation of the Cassini division in Saturn's rings. *Icarus* **34,** 240–253.

GOLDREICH, P., AND S. TREMAINE 1979. Towards a theory for the uranian rings. *Nature* **277,** 97–99.

GOLDREICH, P., AND S. TREMAINE 1982. The dynamics of planetary rings. *Annu. Rev. Astron. Astrophys.* **20,** 249–283.

HÄNNINEN, J. 1993. Numerical simulations of Moon–ringlet interaction. *Icarus* **103,** 104–123.

HÄNNINEN, J., AND H. SALO 1992. Collisional simulations of Satellite Lindblad resonances. *Icarus* **97,** 228–247.

HÄNNINEN, J., AND H. SALO 1994. Collisional simulations of Satellite Lindblad resonances. II. Formation of narrow ringlets. *Icarus* **108,** 325–346.

PORCO, C., AND P. NICHOLSON 1987. Eccentric features in Saturn's outer C-ring. *Icarus* **72,** 437–467.

ROSEN, P. A., G. L. TYLER, E. A. MAROUF, AND J. J. LISSAUER 1991. Resonance structures in Saturn's rings probed by radio occultation. *Icarus* **93,** 25–44.

SALO, H. 1991. Numerical simulations of dense collisional systems. *Icarus* **90,** 254–270.

SALO, H. 1992. Gravitational wakes in Saturn's rings. *Nature* **359,** 619–621.

SCHWARZ, M. P. 1981. Clearing the Cassini division. *Icarus* **48,** 339–342.

SHU, F. 1984. Waves in planetary rings. In *Planetary Rings* (R. Greenberg and A. Brahic, Eds.), pp. 513–561. Univ. of Arizona Press, Tucson.

TYLER, G. L., E. A. MAROUF, R. A. SIMPSON, H. A. ZEBKER, AND R. ESHLEMAN 1983. The microwave opacity of Saturn's rings at wavelengths of 3.6 and 13 cm from Voyager 1 radio occultation. *Icarus* **54,** 160–188.